NANO LETTERS

pubs.acs.org/NanoLett

Letter

Heparin-Induced Allosteric Changes in SARS-CoV-2 Spike Protein Facilitate ACE2 Binding and Viral Entry

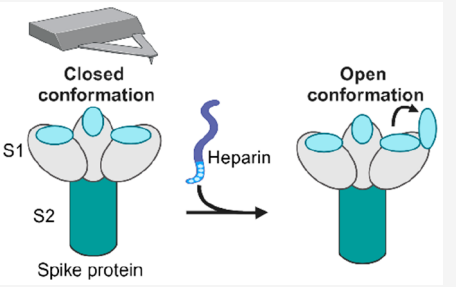
Simon J. L. Petitjean,[3] Savannah Eeckhout,[3] Martin Delguste, Qingrong Zhang, Kimberley Durlet, and David Alsteens*

Cite This: *Nano Lett.* 2023, 23, 11678−11684

Read Online

ACCESS | Metrics & More | Article Recommendations | Supporting Information

ABSTRACT: Understanding the entry of severe acute respiratory syndrome-coronavirus-2 (SARS-CoV-2) into host cells is crucial in the battle against COVID-19. Using atomic force microscopy (AFM), we probed the interaction between the virus's spike protein and heparan sulfate (HS) as a potential attachment factor. Our AFM studies revealed a moderate-affinity interaction between the spike protein and HS on both model surfaces and living cells, highlighting HS's role in early viral attachment. Remarkably, we observed an interplay between HS and the host cell receptor angiotensin-converting enzyme 2 (ACE2), with HS engagement resulting in enhanced ACE2 binding and subsequent viral entry. Our research furthers our understanding of SARS-CoV-2 infection mechanisms and reveals potential interventions targeting viral entry. These insights are valuable as we navigate the evolving landscape of viral threats and seek effective strategies to combat emerging infectious diseases.



KEYWORDS: *SARS-CoV-2, heparin, ACE2, viral entry, atomic force microscopy*

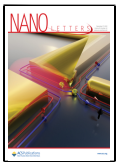
Downloaded via UNIV CATHOLIQUE DE LOUVAIN on January 16, 2024 at 19:59:56 (UTC).
See https://pubs.acs.org/sharingguidelines for options on how to legitimately share published articles.

These past few years have illustrated the major threat that viruses pose to human health and societies in general. Indeed, the severe acute respiratory syndrome-coronavirus-2 (SARS-CoV-2) pandemic caused significant socioeconomic damage as well as more than 6.9 million deaths and 770 million cases[1] reported worldwide in August 2023. Even today, new immunity-evading variants of SARS-CoV-2 are emerging.[2] In addition, SARS-CoV-2 is the third member of the (β-)CoV family to cause an outbreak of infection in human populations in recent years. More than 8000 people have been infected by SARS-CoV since 2003, with a case-fatality rate of ∼10%,[3,4] while Middle East respiratory syndrome (MERS)-CoV has infected more than 1700 people, with a case-fatality rate of ∼36%, since 2012. Thus, with the current SARS-CoV-2 pandemic still ongoing and the possible emergence of new CoV or SARS-CoV-2 variants in the future, it is critical to understand the molecular details underlying viral infection to be able to combat it.

The outcome of a successful viral infection in a target cell largely depends on the ability of the virus to establish early interactions with host cell surface components.[5] When landing on a cellular surface, a virus encounters a wide variety of cell membrane components that are all potentially keen to interact with its surface proteins. One can distinguish entry receptors from attachment factors whose engagement is unspecific and rather weak, mainly allowing the concentration of viral particles at the cellular surface and determining the viral lateral diffusion to specific entry receptors.[6] Although a consensus has been reached on the central role of the angiotensin-converting enzyme 2 (ACE2) receptor in SARS-CoV-2 infection,[7−9] it is becoming increasingly clear that it is not alone in the game and is supported by other surface components.[10−12] The SARS-CoV-2 spike glycoprotein (S), particularly its S1 domain, is showing growing versatility, offering numerous opportunities to interact with specific molecules on the cell surface, notably, certain glycans. After cell membrane binding, SARS-CoV-2 can be internalized following two different pathways:[13,14] either the spike undergoes proteolytic activation mediated by the transmembrane protease serine 2 (TMPRSS2) leading to the release of a fusion peptide and membrane fusion, or the virion is endocytosed and escapes the endosome thanks to other proteases, notably from the cathepsin family.

In this study, we focused on heparan sulfate (HS), a highly negatively charged linear polysaccharide,[15] to determine whether it could serve as an attachment factor for SARS-CoV-2, facilitating the infection process or not. HS is part of the glycocalyx, a dense meshwork of glycans and glycoconjugates surrounding the cell, that participates in several functions such as cell membrane integrity, adhesion, and mechanosensing.[16−18] Because of its high degree of exposure to the cell

Received: September 15, 2023
Revised: December 1, 2023
Accepted: December 1, 2023
Published: December 6, 2023



ACS Publications

© 2023 American Chemical Society

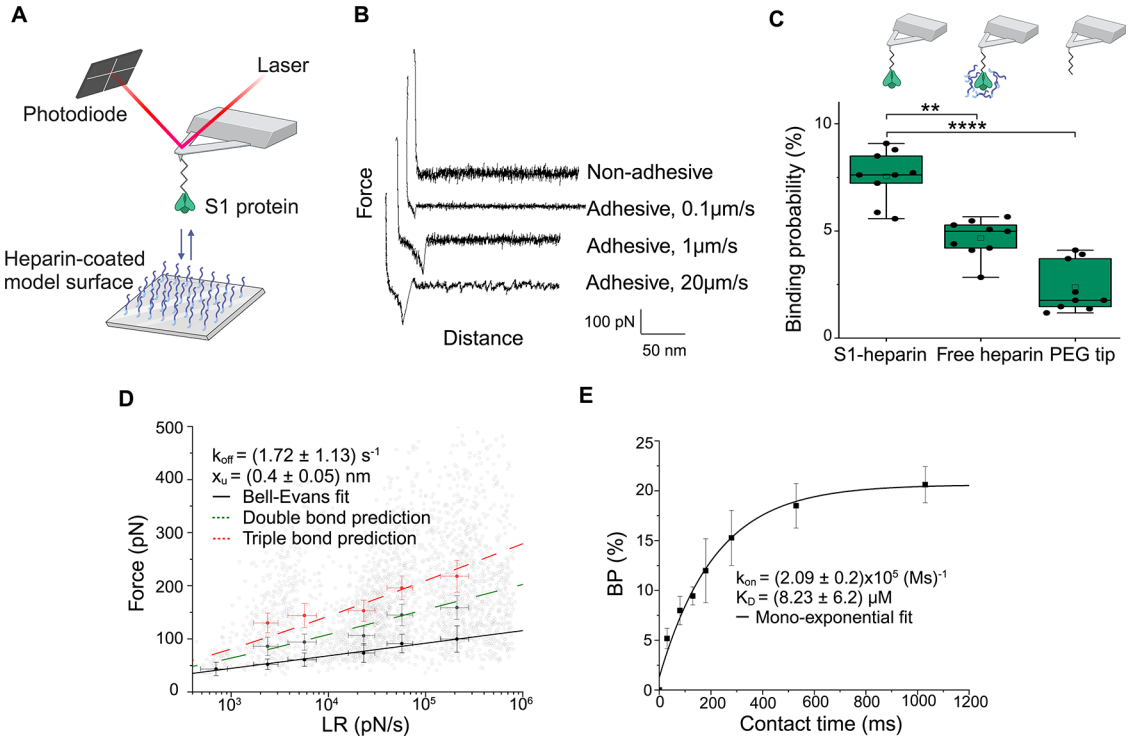


Figure 1. Exploring the SARS-CoV-2−heparin interaction dynamics on model surfaces. (A) The interaction of S1 protein with heparin is probed using FD curve-based AFM on model surfaces. (B) Representative retraction parts of FD curves recorded while probing the S1−heparin interaction at different pulling speeds. (C) Box plot showing the binding probability measured by AFM for the S1−heparin interaction, the S1−heparin interaction when free heparin is injected in the medium, and the S1−heparin interaction when the AFM tip is functionalized with only a PEG linker (from left to right, respectively). One data point corresponds to the binding probability (BP) from one map acquired at a retraction speed of 1 μm/s. The square in the box indicates the mean; the colored box indicates the 25th and 75th percentiles, and the whiskers indicate the highest and lowest values. The line in the box indicates the median. N = 9 maps examined over three independent experiments. p values were calculated using GraphPad Prism. A Wilcoxon test was performed for the effect of heparin injection, whereas the PEG tips were compared to the S1 tips with a Mann−Whitney test: $^{**}p < 0.01$; $^{****}p < 0.0001$. (D) Dynamic force spectroscopy (DFS) plot describing the S1−heparin interaction. The distribution of rupture forces measured as a function of the LR (gray dots, each one corresponding to a force−LR couple extracted from an FD curve; N = 2539 from six independent experiments) is presented. The average rupture force of the single interaction (black dots) is determined for six distinct LR ranges and fitted with the Bell−Evans fit (straight black line), leading to the extraction of the kinetic off-rate (k_{off}) and distance to the transient state (x_u) values. The same procedure was applied for double (green) and triple (red) interactions that are compared to the Williams−Evans predictions (dashed lines). See also Figure S1. (E) Plot of the BP as a function of contact time for the S1−heparin interaction. Each point represents the mean of three independent maps acquired at a retraction speed of 1 μm/s for each contact time, and the data are fitted using a least-squares fit of monoexponential growth (black line). Panel A and the insets of panel C were created with Biorender.

surface and its spatial arrangement, many viruses (such as influenza,[19] herpes,[20,21] etc.) have used it as their first foothold.

Recent data indicate that SARS-CoV-2 can interact with HS through its S protein. The receptor-binding domain (RBD) binds heparin with an affinity in the micromolar range, whereas the full-length S protein has an affinity in the nanomolar range, suggesting the presence of multiple binding sites.[22] Heparin binding, shown to have a nanomolar affinity for the RBD alone in another study, could also promote subsequent ACE2 binding,[23] possibly through a conformational change within the RBD toward an open conformation as suggested by circular dichroism spectroscopy.[24] However, the same study also demonstrated that heparin could prevent SARS-CoV-2 infection, which seems contradictory to the enhancement of ACE2 binding.

Therefore, to better understand the role of HS in the infection process of SARS-CoV-2 and to clarify the conflicting data, we used force−distance (FD) curve-based atomic force microscopy (AFM)[25,26] to investigate the role of heparin in SARS-CoV-2 binding and infection. First, we characterized the bond strength and its kinetic parameters at the single-molecule level (Figure 1. We showed on both model surfaces and living cells that SARS-CoV-2 S1 binds to heparin with a moderate affinity and observed an allosteric role in the formation of the RBD−ACE2 complex. Then, infectivity assays using propagation-incompetent G-deleted vesicular stomatitis virus (VSV) trans-complemented with the SARS-CoV-2 spike protein (VSV-SARS-CoV-2) confirmed the physiological relevance of our findings.

S1 SPECIFICALLY ENGAGES HEPARIN WITH A MODERATE AFFINITY ON MODEL SURFACES

Our initial investigation focused on examining the binding properties of SARS-CoV-2 with heparin, a polysaccharide closely related in structure to HS, at the single-molecule level using FD curve-based AFM. To achieve this, we employed an AFM tip functionalized with the S1 protein via a heterobifunctional linker.[25,26] This modified AFM tip was systematically approached and retracted from a gold-coated surface, where heparin had been immobilized. This immobilization was facilitated through a three-layer setup that harnessed the strong interaction between biotin and streptavidin (for detailed

https://doi.org/10.1021/acs.nanolett.3c03550
Nano Lett. 2023, 23, 11678−11684

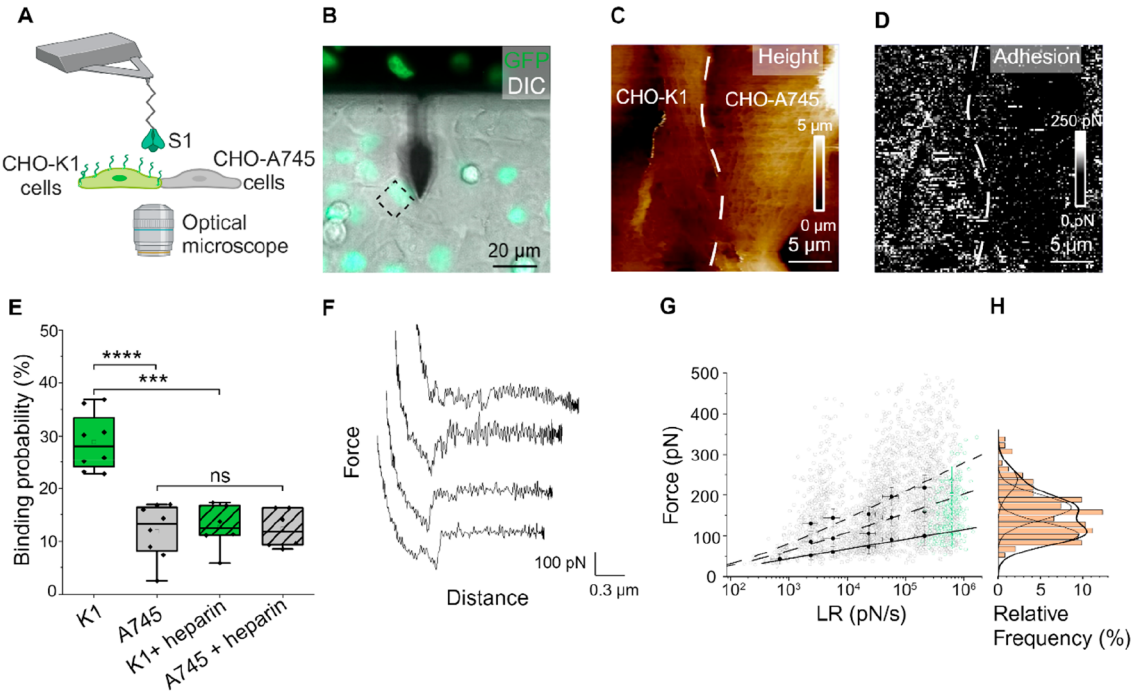


Figure 2. Probing S1−HS interaction on living cells. (A) The interaction of S1 protein with heparin is probed using FD curve-based AFM on a co-culture of HS-expressing (CHO-K1) and non-HS-expressing (CHO-A745) living cells. (B) Overlay of GFP and DIC images of a co-culture of CHO-A745 and fluorescently labeled CHO-K1 cells. The inset shows the area imaged. (C) Height and (D) corresponding adhesion images were recorded using FD curve-based AFM. (E) Box plot showing the binding probability measured by AFM for the S1−CHO-K1 interaction (N= 8), the S1−CHO-A745 interaction (N = 8), the S1−CHO-K1 interaction when free heparin is injected into the medium (N = 6), and the S1−CHO-A745 interaction when free heparin is injected into the medium (N = 6) (from left to right, respectively). One data point belongs to the BP from one map. Three independent experiments were performed. The square in the box indicates the mean; the colored box indicates the 25th and 75th percentiles, and the whiskers indicate the highest and lowest values. The line in the box indicates the median. p values were calculated using GraphPad Prism. An unpaired t test was performed to compare the CHO-K1 cells to CHO-A745 cells. Paired t tests were performed to evaluate the effect of heparin addition: ns = nonsignificant; ***$p < 0.001$; ****$p < 0.0001$. (F) Representative retraction parts of force−distance curves recorded while probing the living cells. (G) DFS plot showing the distribution of the rupture forces measured between the S1 subunit and heparin on model surfaces (black dots, extracted from Figure 1D) and between the S1 subunit and HS-expressing CHO-K1 cells (green dots) (N = 242). The error bar indicates the standard deviation of the mean value. (H) Histograms of force distribution corresponding to the data presented in panel G. Panel A was created with BioRender.

information, see Material and Methods in the Supporting Information and Figure 1A). The purpose of these experiments was to record FD curves, pixel by pixel, across a predefined area of the sample.

FD curves were collected and then sorted on the basis of the presence of a specific adhesion peak (i.e., following the worm-like chain model[27] for protein extension) in the retraction part (Figure 1B), and we calculated the binding probability (BP) as the ratio of specific adhesion events to the total number of curves. A BP of ∼8% was measured between S1 and heparin, suggesting that the two partners effectively bind. To confirm the specificity of the interaction, we performed two independent controls. We observed a significant reduction in binding propensity, evidenced by a notable decrease in the measured BP, under two distinct conditions: (1) when the S1 protein was probed in the presence of free heparin (25 μg/mL) in the medium, a situation in which free heparin molecules competed for binding sites with the S1 protein, and (2) when a tip functionalized solely with the PEG linker was employed (Figure 1C).

Next, we explored the free-energy landscape of the interaction by extracting its kinetic off-rate (k_{off}), distance to the transient state (x_u), and kinetic on-rate (k_{on}). In the first step, we performed dynamic force spectroscopy (DFS) experiments to investigate the bond's dissociation properties. The Bell−Evans model[28−30] states that the energy barrier is dependent on the loading rate (LR), i.e., on how fast we pull on the bond. We, therefore, collected rupture forces over a wide range of LRs (by varying the retraction speed of the tip) and plotted them in a so-called DFS plot (Figure 1D). Analysis of the rupture force distribution for different LR ranges allowed us to identify the different existing force populations (Figure S1).[31,32] The data corresponding to the single S1−heparin binding (black dots in Figure 1D) were fitted with the Bell−Evans model, leading to the extraction of a k_{off} of 1.72 ± 1.13 s^{-1} and an x_u of 0.40 ± 0.05 nm. On the basis of these results, we drew the Williams−Evans prediction for uncorrelated bonds loaded in parallel and compared it with our multivalent force populations. This analysis highlights that up to three bonds are occurring simultaneously.

Next, we studied the rate of association of the S1−heparin complex.[31,33] In other words, we measured the binding probability as a function of the contact time between the tip and the sample (Figure 1E). The data were fitted with a monoexponential fit to extract the interaction time, assuming pseudo-first-order kinetics. Approximating that the interaction can take place in a volume corresponding to a half-sphere whose radius encompasses the PEG linker, the S1 protein, and heparin, we calculated a k_{on} of (2.09 ± 0.2) × 10^5 M^{-1} s^{-1}. Finally, putting these results together, we calculated an affinity

https://doi.org/10.1021/acs.nanolett.3c03550
Nano Lett. 2023, 23, 11678−11684

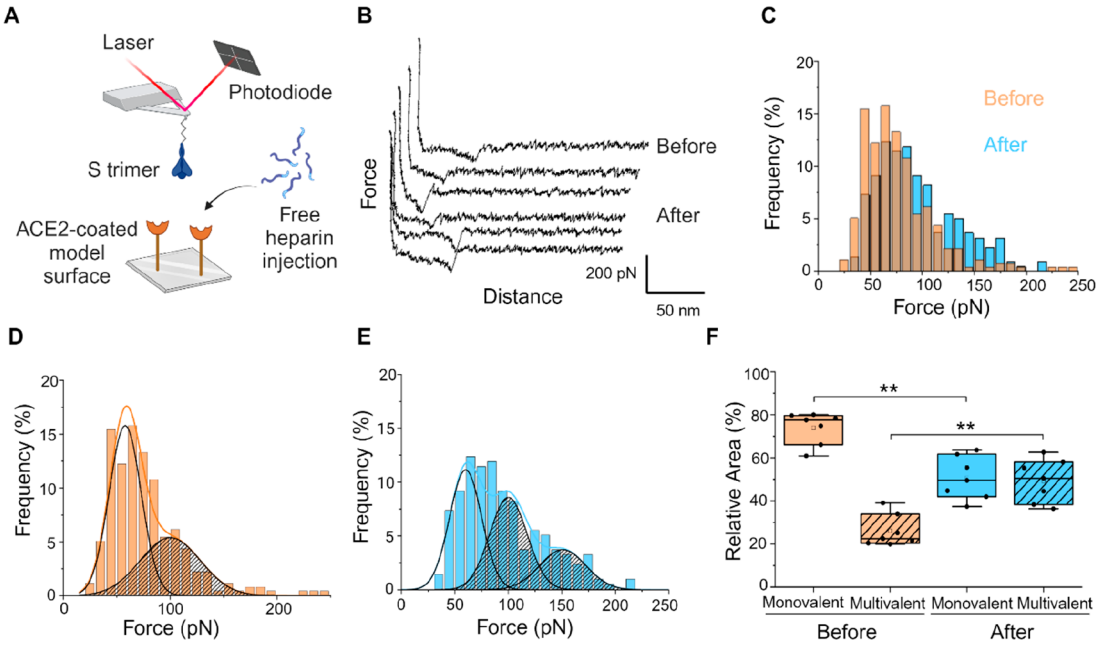


Figure 3. Monitoring the effect of heparin on the S−ACE2 interaction. (A) Effect of heparin on the S−ACE2 interaction probed using FD curve-based AFM. (B) Representative retraction parts of FD curves recorded at a pulling speed of 1 μm/s while probing the S−ACE2 interaction before and after heparin injection. (C) Overlay of the force distribution histograms before (light orange) and after (light blue) heparin injection for a single retraction speed (N = 279 and 219 before and after heparin injection, respectively, from four different independent experiments). See also Figure S3. Force distribution histograms (D) before and (E) after heparin injection. The curves represent Gaussian fits that enable the identification of different force populations. The hatched areas correspond to multivalent forces. (F) Box plot showing the occurrence of monovalent and multivalent interactions before and after the injection of heparin. One data point represents the relative area measured at one pulling speed. Three independent experiments were performed for each of the seven speeds. The square in the box indicates the mean; the colored box indicates the 25th and 75th percentiles, and the whiskers indicate the highest and lowest values. The line in the box indicates the median. p values were calculated using paired t tests on GraphPad Prism: $^{**}p < 0.01$. Panel A was created with Biorender.

constant K_D of 8.23 ± 6.2 μM by calculating the ratio of the kinetic constants.

THE INTERACTION IS PHYSIOLOGICALLY RELEVANT

Our initial findings were subsequently corroborated through experiments conducted on living cells, which offer a more physiologically relevant context by presenting a diverse array of surface molecules to which SARS-CoV-2 can bind. The study involved a co-culture system comprising CHO-K1 (WT) and CHO-A745 (HS non-expressing mutant, utilized as a direct internal control) cell lines (Figure 2A). These cells were maintained alive under physiological conditions (37 °C, humidified air complemented with 5% CO_2) during the whole experiment. Using fluorescence signals, CHO-K1 cells expressing the green fluorescence protein (GFP) were distinctly identified as green. An imaging approach was adopted to capture an area encompassing both cell lines, facilitating a direct comparison of their respective binding properties (Figure 2B−D and Figure S2), probed using a S1-functionalized tip.

The results obtained from our experiments reveal a significantly higher binding affinity for WT cells than for mutant cells (Figure 2E). Intriguingly, we observed that the binding level on WT cells could be significantly reduced to a degree comparable to that observed for the mutant cells by introducing free heparin (0.5 mg/mL) into the medium, as depicted in Figure 2E. Conversely, no discernible effect on the mutant cell line was observed under the same conditions.

In addition, we performed a full analysis of the FD curves (Figure 2F−H). This examination revealed a remarkable alignment on the DFS plot between the force recorded on the CHO-K1 cells (green circles) and the data previously acquired on the model surfaces (gray circles). This agreement is further validated by the force histogram (Figure 2H), which highlights the presence of local maxima that correspond closely to the distribution observed on model surfaces. The remarkable agreement between these two data sets underscores the specific nature of the heparin−SARS-CoV-2 interaction during the probing of CHO-K1 cells. Moreover, it implies that the kinetics governing this interaction on model surfaces closely mimic those observed in a cellular context. Together, these findings substantiate our assertion that our investigations indeed target a specific heparin−SARS-CoV-2 interaction on WT cells and this interaction on model surfaces faithfully reproduces the dynamic behavior witnessed within a cellular environment.

HEPARIN PROMOTES ACE2 BINDING

With the establishment and characterization of the S1−heparin interaction, an intriguing question arises concerning its potential role in the infection process. Existing reports[23,24] have indicated that ACE2 binding by the RBD is facilitated when it adopts an open conformation. It is plausible that heparin could act as a promoter, inducing the transition from the closed to the open conformation and thus influencing the infection dynamics.

We systematically investigated this phenomenon by utilizing our FD curve-based AFM approach. To examine the influence

https://doi.org/10.1021/acs.nanolett.3c03550
Nano Lett. 2023, 23, 11678−11684

of heparin, we employed an ACE2 model surface and probed it by using an S trimer-functionalized AFM tip. These experiments were conducted both before and after the introduction of 0.5 mg/mL free heparin into the medium (Figure 3A). Utilizing the full S trimer allowed us to better evaluate the potential multivalency of the interaction and enabled us to observe conformational transitions within the S trimer. Notably, both scenarios (before and after heparin injection) exhibited similar FD curve profiles (Figure 3B).

Subsequently, we plotted the force distributions for various pulling speeds and observed an increase in higher force values following heparin injection (depicted in blue with an example for one pulling speed presented in Figure 3C; full data available in Figure S3). By employing Gaussian analysis of the histograms (Figure 3D,E), we noted that different force populations clustered around similar force values. However, heparin injection promoted multivalent interactions, as indicated by the hatched areas in the histograms (Figure 3E). The triple bond interactions were exclusively detectable post-injection (Figure 3E). We quantified this shift for all pulling speeds by calculating the respective peak areas and deduced a significant reduction in the number of monovalent interactions in favor of multivalent interactions, as presented in Figure 3F.

HEPARIN INCREASES INFECTIVITY

Following the observation that heparin induces a stronger multivalent interaction with the ACE2 host receptors (Figure 3F), we sought to explore the implications of these enhanced binding properties for the infectivity of SARS-CoV-2. To investigate this, we conducted infectivity assays under controlled biosafety conditions, involving A549 lung carcinoma cells expressing ACE2 and TMPRSS2 (A549 ACE2 TMPRSS2). These cells were incubated with VSV-SARS-CoV-2, which encodes a GFP reporter protein. First, we confirmed the involvement of heparin in SARS-CoV-2 infection by subjecting cells to heparinase treatment, resulting in the removal of HS from the cell surface. This treatment correlated with a significant reduction of 26.4 ± 11.4% (N = 3) in infectivity when compared to that of the positive control (CT+), which did not undergo heparinase treatment (Figure 4). Next, we explored the impact of heparin on ACE2 binding by preincubating VSV-SARS-CoV-2 with varying concentrations of free heparin, ranging from 0.075 to 1 mg/mL. This concentration range encompassed 0.5 mg/mL used in our AFM experiments. Subsequently, we injected the mixture onto A549 ACE2 TMPRSS2 cells. Our findings, as illustrated in Figure 4, indicate a dose-dependent effect of heparin on infection efficiency. The highest concentration (1 mg/mL) significantly increased VSV-SARS-CoV-2 infectivity by 31.6 ± 16.7% (N = 3). In contrast, the lowest concentration (0.075 mg/mL) of heparin resulted in a slight decrease in infectivity efficiency, with a 25.3 ± 16.1% (N = 3) reduction. Taken together, these results support the hypothesis that heparin, by enhancing binding to ACE2, plays a role in cell infectivity.

HS has been shown in the past to be used by many other viruses[17,34] (including herpes simplex virus[35] and dengue virus[36]) as an attachment factor for viral infection, meaning that its engagement usually serves as a first (relatively) nonspecific point of anchorage without actively triggering infection.[37] This presupposed role of an attachment factor is usually associated with a moderate-affinity interaction, as the virus must be able to move on the cellular surface to search for its specific entry receptor (ACE2 in the case of SARS-CoV-2). Here, our single-molecule approach yielded a micromolar affinity, thus in line with the previous statement, but in contradiction to other ensemble studies.[22,23] However, the latter tend to underestimate the kinetic off-rate due to rebinding and multivalence,[38,39] which could explain the discrepancy observed in the results, especially as complete viruses and large polymeric molecules like heparin favor multiplicity.

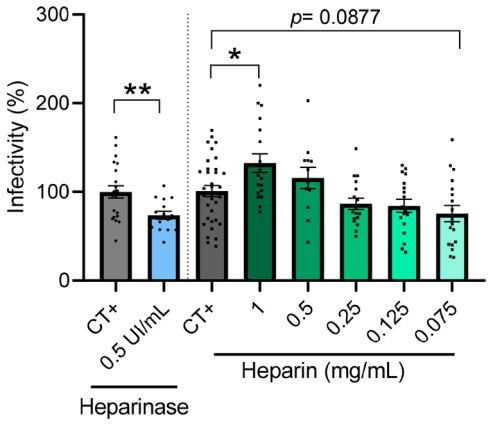


Figure 4. Infectivity assay with heparinase or heparin injection. On the left of the bar chart is shown the effect of heparinase incubation with A549 ACE2 TMPRSS2 cells before VSV-SARS-CoV-2 infection. On the right is shown the effect of incubation of VSV-SARS-CoV-2 and depleting concentrations (1, 0.5, 0.25, 0.125, and 0.075 mg/mL) of free heparin on the subsequent infection of A549 ACE2 TMPRSS2 cells. Positive control cells served as the 100% reference for both assays. The values presented are the result of three biological replicates. Each condition usually had six technical replicates, and the positive controls had 12 technical replicates. Outliers were treated with the Grubbs method. A single data point corresponds to one technical replicate, i.e., the fluorescent signal of one well. Overall data point numbers per condition range from 12 to 34. p values were calculated using GraphPad Prism. An unpaired t test was performed to assess the impact of heparinase. A one-way analysis of variance and Dunnett's multiple-comparison test were performed to evaluate the effect of heparin addition: ns = nonsignificant; *$p < 0.05$; **$p < 0.01$. Errors bars represent the standard error of the mean.

We subsequently delved into the potential interaction between HS and ACE2 binding, as prior research established that SARS-CoV-2 engagement with HS triggers a conformational change in the RBD, shifting it toward an open conformation that promotes subsequent ACE2 binding.[23,24] Our study unveiled a significant enhancement in ACE2 binding when HS is present, as evidenced by the observation of larger binding forces. In terms of mechanisms, our investigation revealed that this enhancement correlates with an increase in the frequency of multivalent interactions, which collectively reinforce the overall binding strength.

This intricate interplay, suggesting a pivotal role at the intersection of a specific receptor (ACE2) and an attachment factor (HS), is a phenomenon that has not been extensively documented in previous research. A notable parallel can be drawn to the sialic acid−junctional adhesion molecule-A (JAM-A) interaction observed in reovirus,[40,41] further emphasizing the significance of such multifaceted interactions in viral infection dynamics

Remarkably, we discovered a positive correlation between stronger binding and infectivity, as the presence of heparin

https://doi.org/10.1021/acs.nanolett.3c03550
Nano Lett. 2023, 23, 11678−11684

(>0.5 mg/mL) significantly boosts the infectivity of VSV-SARS-CoV-2. These findings stand in contrast to previous research,[23,24,42] which suggests that despite its physiological function, heparin can inhibit SARS-CoV-2 infection. A notable distinction we observed is that the majority of these studies utilized cell lines lacking the expression of TMPRSS2, namely, Vero E6,[13] H1299,[43] and A549[13] cell lines. It is worth recalling that TMPRSS2, positioned on the cell membrane, plays a fundamental role in determining the entry pathway of SARS-CoV-2. When TMPRSS2 is present, it cleaves the spike protein after ACE2 binding, thereby exposing the hydrophobic fusion peptide responsible for initiating direct membrane fusion. If not, SARS-CoV-2 virions remain anchored to the cell membrane until endocytosis takes place, and they eventually escape the endosome thanks to the activity of other intracellular proteases, notably cathepsin L.[13,14] Therefore, the role of HS in the infectivity of SARS-CoV-2 could depend on the presence and activity of TMPRSS2. It could also depend on the SARS-CoV-2 variants, as it has been shown that the latest omicron variant tends to use multiple entry routes compared to the WT virus.[43,44]

In light of heparin's interaction with ACE2 causing a potential increase in infectivity, a crucial question about its therapeutic potential as a blocking agent remains. It should be noted that heparin possesses valuable anticoagulant properties, making it an optimal candidate for improving the circulatory system and reducing the incidence of venous thromboembolism in critically ill patients with COVID-19. Endogenous plasma heparin levels in humans range from 1 to 2.4 mg/L,[45] and doses of ≤2 mg/kg[46] were administered to COVID-19 patients. These levels remain within the range of the low concentration that we tested, for which we did not observe an increase in infectivity. However, at the cell surface of our epithelial cells, the local concentration of heparan sulfate could be significantly higher, potentially playing a pivotal role in initiating virus activation during the initial binding stages.[47−49]

Overall, our findings highlight the need for a broader understanding of attachment factors in the viral invasion dynamics. While we illuminate how the role of a single attachment factor can substantially affect infection, information about how multiple attachment factors collectively impact the latter is still lacking. Larger studies are needed to fully decipher the intricacies of viral ingress.

■ ASSOCIATED CONTENT

Supporting Information

The Supporting Information is available free of charge at https://pubs.acs.org/doi/10.1021/acs.nanolett.3c03550.

Material and Methods, probing the binding of S1 to heparin on a model surface (Figure S1), probing the binding of S1 to heparin on living cells (Figure S2), and monitoring the effect of heparin on ACE2 binding (Figure S3) (PDF)

■ AUTHOR INFORMATION

Corresponding Author

David Alsteens − *Louvain Institute of Biomolecular Science and Technology, Université catholique de Louvain, Louvain-la-Neuve, Walloon Brabant 1348, Belgium; WELBIO Department, WEL Research Institute, Wavre, Walloon Brabant 1300, Belgium;* orcid.org/0000-0001-9229-113X; Email: david.alsteens@uclouvain.be

Authors

Simon J. L. Petitjean − *Louvain Institute of Biomolecular Science and Technology, Université catholique de Louvain, Louvain-la-Neuve, Walloon Brabant 1348, Belgium*

Savannah Eeckhout − *Louvain Institute of Biomolecular Science and Technology, Université catholique de Louvain, Louvain-la-Neuve, Walloon Brabant 1348, Belgium*

Martin Delguste − *Louvain Institute of Biomolecular Science and Technology, Université catholique de Louvain, Louvain-la-Neuve, Walloon Brabant 1348, Belgium*

Qingrong Zhang − *Louvain Institute of Biomolecular Science and Technology, Université catholique de Louvain, Louvain-la-Neuve, Walloon Brabant 1348, Belgium*

Kimberley Durlet − *Louvain Institute of Biomolecular Science and Technology, Université catholique de Louvain, Louvain-la-Neuve, Walloon Brabant 1348, Belgium*

Complete contact information is available at: https://pubs.acs.org/10.1021/acs.nanolett.3c03550

Author Contributions

[3]S.J.L.P. and S.E. contributed equally to this work.

Notes

The authors declare no competing financial interest.

■ ACKNOWLEDGMENTS

This work was supported by the Université catholique de Louvain, the Foundation Louvain, and the Fonds National de la Recherche Scientifique (F.R.S.-FNRS) under the Excellence of Science (EOS) program (Grant 40007527). This project received funding from the European Research Council under the European Union's Horizon 2020 research and innovation program (Grant Agreement 758224) and from the FNRS-Welbio (Grant CR-2019S-01). The funders had no role in study design, data collection and analysis, decision to publish, or preparation of the manuscript. S.J.L.P. and S.E. are Research Fellow at F.R.S.-FNRS, and D.A. is Senior Research Associate at F.R.S.-FNRS. The TOC image was created using Biorender.com.

■ REFERENCES

(1) WHO Coronavirus (COVID-19) Dashboard. https://covid19.who.int (accessed 2023-09-01).

(2) McCallum, M.; et al. SARS-CoV-2 immune evasion by the B.1.427/B.1.429 variant of concern. *Science* **2021**, *373*, 648−654.

(3) Ksiazek, T. G.; et al. A novel coronavirus associated with severe acute respiratory syndrome. *N. Engl. J. Med.* **2003**, *348*, 1953−1966.

(4) Florindo, H. F.; et al. Immune-mediated approaches against COVID-19. *Nat. Nanotechnol.* **2020**, *15*, 630−645.

(5) Grove, J.; Marsh, M. The cell biology of receptor-mediated virus entry. *J. Cell Biol.* **2011**, *195*, 1071−1082.

(6) Smith, A. E.; Helenius, A. How viruses enter animal cells. *Science* **2004**, *304*, 237−242.

(7) Yang, J.; et al. Molecular interaction and inhibition of SARS-CoV-2 binding to the ACE2 receptor. *Nat. Commun.* **2020**, *11*, 4541.

(8) Yan, R.; et al. Structural basis for the recognition of SARS-CoV-2 by full-length human ACE2. *Science* **2020**, *367*, 1444−1448.

(9) Verdecchia, P.; et al. The pivotal link between ACE2 deficiency and SARS-CoV-2 infection. *Eur. J. Int. Med.* **2020**, *76*, 14−20.

(10) Evans, J. P.; Liu, S.-L. Role of host factors in SARS-CoV-2. *entry. J. Biol. Chem.* **2021**, *297*, No. 100847.

(11) Jackson, C. B.; et al. Mechanisms of SARS-CoV-2 entry into cells. *Nat. Rev. Mol. Cell Biol.* **2022**, *23*, 3−20.

(12) Baggen, J.; et al. Cellular host factors for SARS-CoV-2 infection. *Nat. Microbiol.* **2021**, *6*, 1219−1232.

(13) Koch, J.; et al. TMPRSS2 expression dictates the entry route used by SARS-CoV-2 to infect host cells. *EMBO J.* **2021**, *40*, No. e107821.
(14) Hoffmann, M.; et al. SARS-CoV-2 cell entry depends on ACE2 and TMPRSS2 and is blocked by a clinically proven protease inhibitor. *Cell* **2020**, *181*, 271−280.e8.
(15) Lindahl, U.; Couchman, J.; Kimata, K.; et al. Proteoglycans and Sulfated Glycosaminoglycans. In *Essentials of Glycobiology*, 3rd ed.; Varki, A., et al., Eds.; Cold Spring Harbor Laboratory Press: Plainview, NY, 2015; Chapter 17. DOI: 10.1101/glycobiology.3e.017
(16) Reitsma, S.; et al. The endothelial glycocalyx: composition, functions, and visualization. *Pflugers. Arch.* **2007**, *454*, 345−359.
(17) Cagno, V.; et al. Heparan sulfate proteoglycans and viral attachment: true receptors or adaptation bias? *Viruses* **2019**, *11*, 596.
(18) Stencel-Baerenwald, J. E.; et al. The sweet spot: defining virus-sialic acid interactions. *Nat. Rev. Microbiol.* **2014**, *12*, 739−749.
(19) Weis, W.; et al. Structure of the influenza virus haemagglutinin complexed with its receptor, sialic acid. *Nature* **1988**, *333*, 426−431.
(20) Delguste, M.; et al. Single-virus force spectroscopy discriminates the intrinsic role of two viral glycoproteins upon cell surface attachment. *Nano Lett.* **2021**, *21*, 847−853.
(21) Delguste, M.; et al. Multivalent binding of herpesvirus to living cells is tightly regulated during infection. *Sci. Adv.* **2018**, *4*, No. eaat1273.
(22) Liu, L.; et al. Heparan sulfate proteoglycans as attachment factor for SARS-CoV-2. *ACS Cent. Sci.* **2021**, *7*, 1009−1018.
(23) Clausen, T. M.; et al. SARS-CoV-2 Infection depends on cellular heparan sulfate and ACE2. *Cell* **2020**, *183*, 1043−1057.e15.
(24) Mycroft-West, C. J.; et al. Heparin inhibits cellular invasion by SARS-CoV-2: structural dependence of the interaction of the spike S1 receptor-binding domain with heparin. *Thromb. Haemost.* **2020**, *120*, 1700−1715.
(25) Viljoen, A.; et al. Force spectroscopy of single cells using atomic force microscopy. *Nat. Rev. Methods Primers* **2021**, *1*, 1−24.
(26) Müller, D. J.; et al. Atomic force microscopy-based force spectroscopy and multiparametric imaging of biomolecular and cellular systems. *Chem. Rev.* **2021**, *121*, 11701−11725.
(27) Bustamante, C.; et al. Entropic elasticity of λ-Phage DNA. *Science* **1994**, *265*, 1599−1600.
(28) Bell, G. I. Models for the specific adhesion of cells to cells. *Science* **1978**, *200*, 618−627.
(29) Evans, E.; Ritchie, K. Dynamic strength of molecular adhesion bonds. *Biophys. J.* **1997**, *72*, 1541−1555.
(30) Evans, E.; et al. Sensitive force technique to probe molecular adhesion and structural linkages at biological interfaces. *Biophys. J.* **1995**, *68*, 2580−2587.
(31) Rankl, C.; et al. Multiple receptors involved in human rhinovirus attachment to live cells. *PNAS.* **2008**, *105*, 17778−17783.
(32) Alsteens, D.; et al. Nanomechanical mapping of first binding steps of a virus to animal cells. *Nat. Nanotechnol.* **2017**, *12*, 177−183.
(33) Rankl, C.; et al. Determination of the kinetic on- and off-rate of single virus-cell interactions. *Methods Mol. Biol. Clifton NJ.* **2011**, *736*, 197−210.
(34) De Pasquale, V.; et al. Heparan sulfate proteoglycans in viral infection and treatment: a special focus on SARS-CoV-2. *Int. J. Mol. Sci.* **2021**, *22*, 6574.
(35) Shukla, D.; et al. A novel role for 3-*O*-sulfated heparan sulfate in herpes simplex virus 1 entry. *Cell* **1999**, *99*, 13−22.
(36) Artpradit, C.; et al. Recognition of heparan sulfate by clinical strains of dengue virus serotype 1 using recombinant subviral particles. *Virus Res.* **2013**, *176*, 69−77.
(37) Jolly, C. L.; Sattentau, Q. J. Attachment factors. *Adv. Exp. Med. Biol.* **2006**, *790*, 1−23.
(38) Papp, I.; et al. Inhibition of influenza virus infection by multivalent sialic-acid-functionalized gold nanoparticles. *Small Weinh. Bergstr. Ger.* **2010**, *6*, 2900−2906.
(39) Newton, R.; et al. Combining confocal and atomic force microscopy to quantify single-virus binding to mammalian cell surfaces. *Nat. Protoc.* **2017**, *12*, 2275−2292.
(40) Koehler, M.; et al. Glycan-mediated enhancement of reovirus receptor binding. *Nat. Commun.* **2019**, *10*, 4460.
(41) dos Santos Natividade, R.; et al. Deciphering molecular mechanisms stabilizing the reovirus-binding complex. *Proc. Natl. Acad. Sci. U. S. A.* **2023**, *120*, No. e2220741120.
(42) Conzelmann, C.; et al. Inhaled and systemic heparin as a repurposed direct antiviral drug for prevention and treatment of COVID-19. *Clin. Med. London Engl.* **2020**, *20*, e218−e221.
(43) Meng, B.; et al. Altered TMPRSS2 usage by SARS-CoV-2 Omicron impacts infectivity and fusogenicity. *Nature* **2022**, *603*, 706−714.
(44) Metzdorf, K.; et al. TMPRSS2 is essential for SARS-CoV-2 Beta and Omicron infection. *Viruses* **2023**, *15*, 271.
(45) Engelberg, H.; et al. Plasma heparin levels in normal man. *Circulation* **1961**, *23*, 578−581.
(46) Bonfim, L. C. M. G.; et al. Optimal dosing of heparin for prophylactic anticoagulation in critically ill COVID-19 patients a systematic review and meta-analysis of randomized controlled trials. *J. Crit. Care* **2023**, *77*, No. 154344.
(47) Gkogkou, E.; et al. Expression profiling meta-analysis of ACE2 and TMPRSS2, the putative anti-inflammatory receptor and priming protease of SARS-CoV-2 in human cells, and identification of putative modulators. *Redox Biol.* **2020**, *36*, No. 101615.
(48) Lukassen, S.; et al. SARS-CoV-2 receptor ACE2 and TMPRSS2 are primarily expressed in bronchial transient secretory cells. *EMBO J.* **2020**, *39*, No. e105114.
(49) Cioccarelli, C.; et al. IL1β Promotes TMPRSS2 Expression and SARS-CoV-2 Cell Entry Through the p38 MAPK-GATA2 Axis. *Front. Immunol.* **2021**, *12*, No. 781352.

https://doi.org/10.1021/acs.nanolett.3c03550
Nano Lett. 2023, 23, 11678−11684